Phys. Status Solidi A **206**, No. 4, 697–703 (2009) / **DOI** 10.1002/pssa.200824291

physica status solidi a
www.pss-a.com
applications and materials science

The effect of growth temperature on physical properties of heavily doped ZnO:Al films

Jongin Hong[**,1], **Hanjong Paik**[**,2], **Hosung Hwang**[3], **Sunghwan Lee**[2], **Andrew J. deMello**[1], **and Kwangsoo No**[*,2]

[1] Department of Chemistry, Imperial College London, South Kensington Campus, London SW7 2AZ, United Kingdom
[2] Department of Material Science and Engineering, KAIST, 373-1 Guseong-dong, Yuseong-gu, Daejeon 305-701, Korea
[3] Semiconductor Device and Material Laboratory, Samsung Advanced Institute of Technology (SAIT), Yongin 446-712, Korea

Received 15 July 2008, revised 22 October 2008, accepted 18 December 2008
Published online 17 March 2009

PACS 68.37.Hk, 68.37.Ps, 68.55.ag, 73.50.–h, 73.61.Ga, 78.20.Ci

[*] Corresponding author: e-mail ksno@kaist.ac.kr, Phone: +82 42 869 4116, Fax: +82 42 869 3310
[**] These authors contributed equally towards this publication.

Heavily-doped ZnO:Al films have been deposited on high temperature stable glass substrates using radio-frequency (RF) magnetron sputtering. The effect of growth temperature on physical properties of the films has been investigated. The microstructure evolved a columnar structure into a granular one with the increase in growth temperature and then a typical honeycomb-type microstructure representing huge grain formation indicating high densification. All Al-doped ZnO films exhibited high optical transparency and the absorption edge shifted to the short wavelength (blue-shift) as the growth temperature increased. The dense microstructure with a high crystallographic quality and large grains evolved at 500 °C enabled us to obtain 2.28×10^{-3} Ω cm and high visible transmittance over 90% even if the ZnO film was doped with an Al content of approximately 5.5 at%.

1 Introduction Transparent conducting oxides (TCOs) have gained much attention in optoelectronic applications including liquid crystal displays, flat panel displays, thin film transistor applications, photovoltaic (PV) cells and electrochromic materials [1–5]. Among them, indium tin oxide (ITO) has predominantly used as a TCO material in practical applications even if it has some drawbacks including high cost, scarcity and toxicity of indium and chemical instability in a reducing atmosphere at high temperature. Fast developments and expansive markets in optoelectronic devices are strongly demanding an alternative of ITO [6].

Recently, zinc oxide (ZnO) and impurity-doped ZnO have been considered as potential candidates to ITO [7–9]. ZnO is an inexpensive material with low toxicity, thermal and chemical stability, and fabrication flexibility in different etching protocols. In addition, it can be used for other functional devices including thin film transistors, surface acoustic wave (SAW) device, piezoelectric transducers and gas sensors [10, 11]. Zinc oxide, which is either non-stoichiometric or doped with donor and acceptor, shows high conductivity [12–14]. The presence of intrinsic defects, such as O vacancies (V_o) and Zn interstitials (Zn_i), allows non-stoichiometric ZnO to have intrinsic n-type conductivity with high electron densities of 10^{21} cm^{-3}. However, the resistivity of ZnO films is not as good as the ITO standard since ZnO native point defects are not efficient donors. Thus, most work focused on an intentionally doped ZnO, such as ZnO:Al (AZO) and ZnO:Ga (GZO). It has stable electrical and optical properties even if at high temperature and in a reducing atmosphere [15]. Nowadays, its resistivity is close to the order of 10^{-5} Ω cm comparable with the lowest resistivity obtainable for ITO. However, such dopant requires a high degree of deposition control to obtain a carrier concentration of the order of 10^{-21} cm^{-3} because of its high reactivity with oxygen [9, 16–18]. The highest conductivity values have been reported at an Al content of 2–3 at% [10, 12–15]. Above a certain level, the excess Al atoms exist in the films as interstitial atoms or segregate into grain boundaries and/or poor crystallized area. They are working as electrically inactive sites and building up an energy barrier limiting the carrier transport.

Herein, we investigated the effect of growth temperature on physical properties of heavily doped ZnO:Al films

by the systematic analysis from microstructure to electrical/optical properties. The films had the Al content of around 6 at% and the carrier concentration above 10^{20} cm^{-3}. The grazing incidence X-ray reflectivity (GIXR) method has been firstly introduced to determine the film density of these Al-doped ZnO films.

2 Experimental Corning eagle 2000 (Samsung Corning, Korea) was used for a substrate. It is stable up to the temperature of 650 °C and so allows us to investigate the effects of high growth temperature on physical properties of AZO films. The substrate was cleaned in sequence by acetone and ethanol in ultrasonic bath and then rinsed by deionized water. All substrates were dried by compressed N_2 gas. The AZO thin films were deposited in pure Ar atmosphere by using radio-frequency (RF) magnetron sputtering with a 2-inch ZnO single ceramic target doped with 3 wt% Al_2O_3. The base pressure prior to deposition was lower than 3×10^{-6} Torr and working pressure of 4×10^{-3} Torr was maintained at a gas flow rate of 20 sccm. The deposition temperature was varied from room temperature (RT) to 500 °C. The deposition rate of 5 nm/min was obtained at RF power of 40 W and the final thickness of all samples was fixed to 200 nm.

The crystallinity of AZO films was evaluated by X-ray diffraction (XRD, RS3000, Rigaku Co.) of θ–2θ and ω-rocking scans using a Cu K_α radiation ($\lambda = 1.542$ nm). High resolution X-ray reflectivity measurement was used to determine film density using a high resolution X-ray diffractometer (X'pert PRO MRD, Philips). Both scanning electron microscopy (SEM, XL30SFEG, Philips) and transmission electron microscopy (TEM, CM20, Philips) were used for microstructure analysis. Auger electron spectroscopy (AES, Scanning Auger Microprobe 4300, Perkin–Elmer) was performed to determine the relative composition of each element in the films. All peaks were indexed using the Ref. [19]. All carbon peaks were eliminated after the third cycle of Ar ion sputtering and then the relative composition of each element was determined without carbon contamination. The transmittance of the films was measured by a UV/VIS spectrometer (UV-3101PC, Shimadzu) in the wavelength range of 300–1100 nm. Resistivity, carrier concentration and mobility were obtained at room temperature by a Hall measurement system based on the van der Pauw method (Ecopia HMS-3000, Bridge Technology). Before the Hall measurement, the ohmic contact of AZO films with indium metal contacts was confirmed.

3 Results and discussion

3.1 Structural properties Figure 1 show XRD patterns of AZO thin films as a function of deposition temperature ranging from room temperature (RT) to 500 °C. All films show a *c*-axis preferred orientation without any detectable secondary phase of Zn, Al and Al_2O_3 and ternary phase of $ZnAl_2O_4$. We speculate that aluminium substitutively replaced zinc, interstitially existed in the ZnO

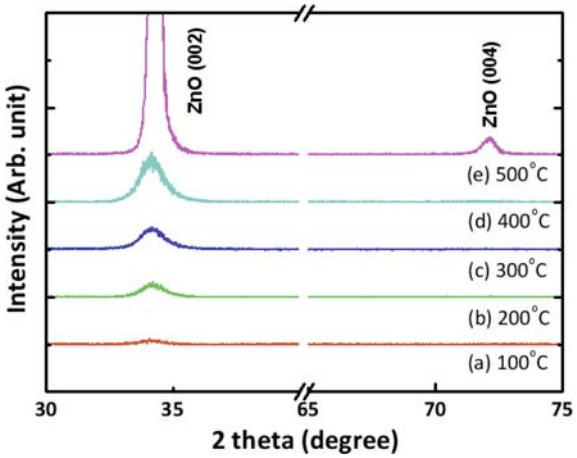

Figure 1 (online colour at: www.pss-a.com) X-ray diffraction patterns of AZO thin films grown at different deposition temperature.

lattice or segregated into the non-crystalline region in grain boundaries. As the temperature increased, the (002) peak intensity increased and the full width at half maximum (FWHM) decreased. Interestingly, in the AZO film deposited at the temperature of 500 °C, the (002) peak was shifted toward higher values. If Al atoms substitute for Zn instead of entering the interstitial site in ZnO, the lattice parameter decreases because the ionic radii of Al^{3+} and Zn^{2+} are 53 pm and 72 pm, respectively. Thus, the (002) peak position shifts toward higher values and it coincides with the observed shift. An Al atom also acts as a donor due to the charge difference between Al^{3+} and Zn^{2+} and thus both electrical and optical properties would be changed significantly. In addition, the appearance of a peak at $2\theta = 72.2°$, which is associated with the (004) plane of the hexagonal phase, means high-quality crystalline structure with a *c*-axis preferred orientation. The average crystallite size parallel to the film surface can be obtained from the analysis of the full width at half maximum (FWHM) and peak position (Table 1). The Debye–Scherer's equation is expressed as

$$d = \frac{0.9\lambda}{\beta \cos\theta}, \tag{1}$$

where d is crystallite size, λ is the wavelength of X-ray, θ is Bragg diffraction angle, β is the full width at half maximum (FWHM). As the deposition temperature increased, the estimated crystallite size increased from 7 nm (at RT) to 19 nm (at 500 °C).

Figure 2 shows SEM images of AZO thin films deposited at different temperatures. The grain size increased with the deposition temperature. The microstructure evolved from a columnar structure into a granular one, and then into a honeycomb-type one as the deposition temperature increased. Above the temperature of 400 °C, we could not distinguish the grain boundaries in the surface images. The typical honeycomb-type surface morphology at the tem-

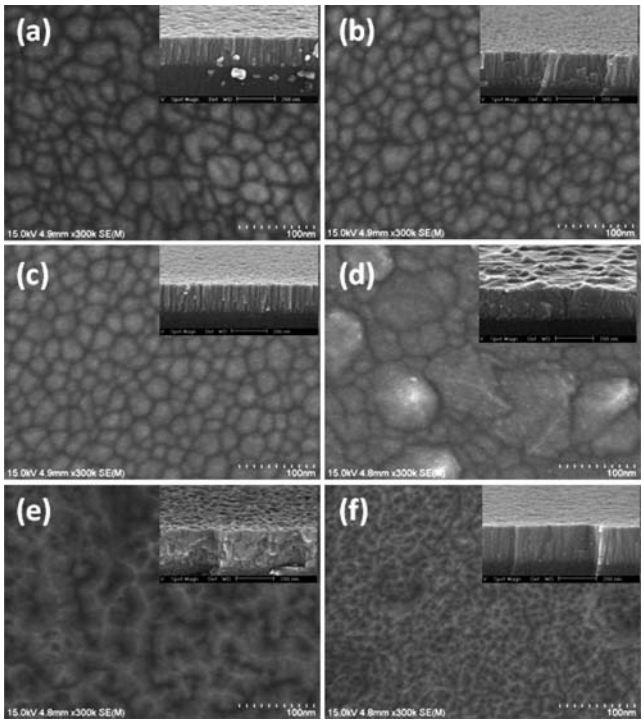

Figure 2 Surface morphology and cross-section of AZO thin films grown at different deposition temperature: (a) R.T., (b) 100 °C, (c) 200 °C, (d) 300 °C, (e) 400 °C, and (f) 500 °C.

perature of 500 °C means huge grain formation and a dense film. We speculate that the microstructure evolution would be strongly related to the movement of surface atoms during the deposition. Thermal energy moves atoms distantly and thus a denser film with large grains and lower defects can be obtained. The TEM analysis of AZO films supports our XRD and SEM observation. The cross-sectional TEM images of ZnO films deposited at RT and 500 °C are shown in Fig. 3(a) and (b), respectively. The apparent columnar-type structure in Fig. 3(a) will result in poor electrical characteristics due to many scattering centers among columns, whilst the continuous-type structure at 500 °C ensure good electrical characteristics. The crystalline quality can also be determined by electron diffraction (ED) patterns. The film deposited at RT had a ring-type arching form indicating polycrystalline nature with small grain size, whilst that deposited at 500 °C had clear spots representing large grains of single crystalline. It should be noted that the quality of AZO films was improved by increasing the deposition temperature.

Figure 4 shows AFM images against deposition temperature. Thin films deposited at the temperature ranging from R.T. to 200 °C were very smooth and the roughnesses were below 3 nm. The films deposited at 300 °C had a relatively rough surface due to partial grain growth and/or abnormal grain coarescence and the roughness was 8.65 nm. Above the temperature of 400 °C, the films showed smooth surfaces. Obviously, the typical honey comb-type surface was very smooth and its roughness was 1.2 nm. These observations coincide with SEM results.

Meanwhile, the grazing incidence X-ray reflectivity (GIXR) enables to estimate the film density (Fig. 5). In the X-ray energy region, the refractive index of a solid medium is lower than that of the air, and thus an X-ray travel-

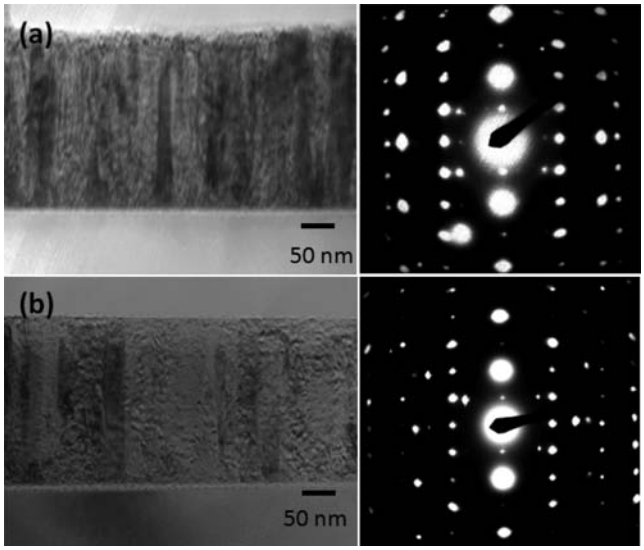

Figure 3 Cross-section image of AZO thin film grown at (a) R.T. and (b) 500 °C, each inset represented electron diffraction patterns at [100] direction.

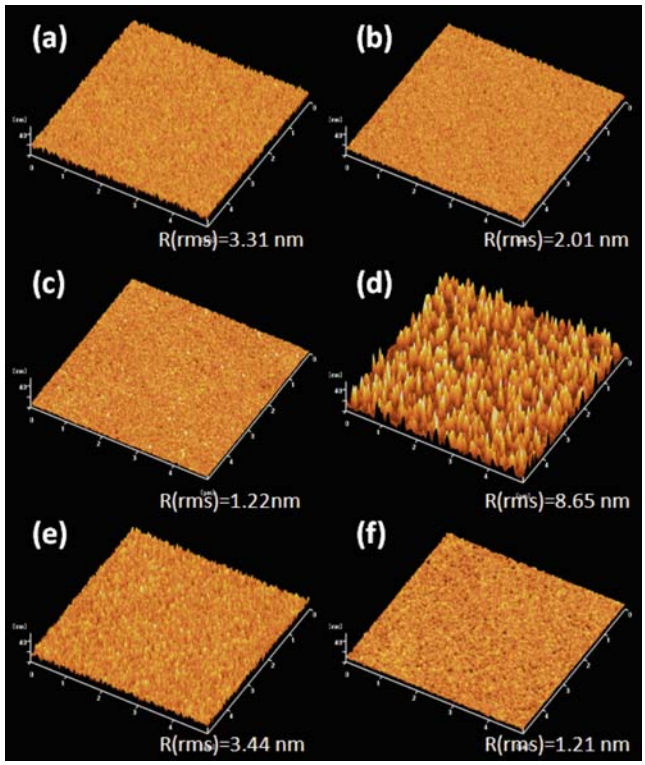

Figure 4 (online colour at: www.pss-a.com) AFM scans against deposition temperature: (a) R.T., (b) 100 °C, (c) 200 °C, (d) 300 °C, (e) 400 °C, and (f) 500 °C.

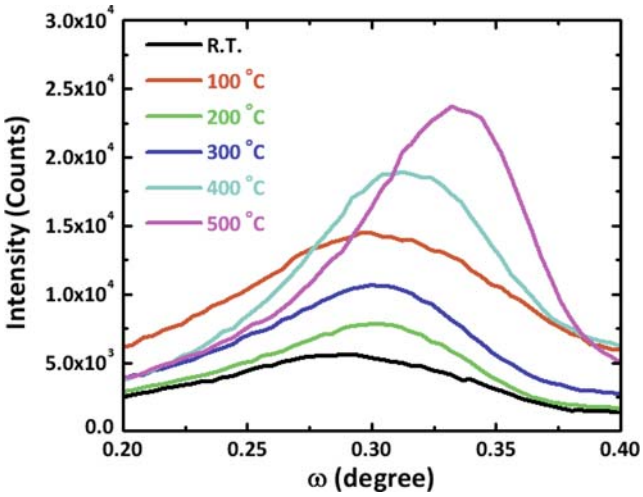

Figure 5 (online colour at: www.pss-a.com) Glancing incident X-ray reflectivity of AZO thin films grown at different deposition temperature from R.T. to 500 °C.

ing in the air, at the proper incident angles, is totally reflected by the medium. The specular reflectivity by $\theta/2\theta$ scan method is obtained by plotting the scattered X-ray intensity against the angle of incidence, θ. The incidence angle beyond, which total reflection is cut off, is referred as the critical angle of total external reflection, θ_c. In the X-ray region, θ_c is generally in the range of tenths of degree and is directly related to the mass density, ρ. The equation can be expressed as [20–22]

$$\frac{\theta_c^2}{\rho} = \frac{r_e \cdot \lambda^2 \cdot Z \cdot N_A}{\pi A} = B\,, \qquad (2)$$

where r_e is the classical electron radius (2.82×10^{-15} m), λ is the wavelength of X-ray, Z is the atomic number, N_A is the Avogadro's number and A is the mass number. B is a unique constant for a given material and irradiating beam. However, it should be noted that the alignment is a compulsory and crucial factor to precisely evaluate a film density. We collected XRR curves at different offset angles and compare them by the maximum scattered (plateau) intensity (called diffuse reflectivity, 'Yoneda' wing [22]). The first peak of the 'Yoneda' wing was normalized and fitted using a Gaussian function. The critical angle increased with the increase in the deposition temperature, and thus higher deposition temperature made the AZO films more densely packed (Table 1).

3.2 Doping concentration and electrical properties Figure 6(a)–(c) show Auger electron spectra of each AZO film deposited at different temperatures and the peak position of each element can be summarized as 997 eV of Zn, 1396 eV of Al and 510 eV of O, respectively. In Fig. 6(d), the AZO films deposited at R.T. and 300 °C had doped Al contents of 6.5 at%, whilst the AZO film deposited at 500 °C had a doped Al content of 5.5 at%. To date, the lowest resistivity could be obtained with the doped Al content of approximately 3.0 at% in the ZnO films because of highest mobility values. Interestingly, Minami et al. reported that the PLD-prepared AZO thin films doped with an Al content of 5–8 at% exhibited the highest resistivity stability in a high humidity environment [23]. The resistivity that they reported is similar with that of our AZO film deposited at 500 °C by using RF magnetron sputtering. Thus, we expect that a heavily doped AZO film with lower resistivity will be of significant importance when used in activated oxidizing environments, such as high temperature and high humidity.

Figure 7 shows physical properties as a function of deposition temperature: (a) the resistivity and film density, (b) carrier mobility and concentration and (c) mean free path and crystallite size. The resistivity decreased with the increase in the growth temperature because of the microstructure evolution and film densification. The resistivity is a function of both carrier concentration and carrier mobility. We think that the increase in carrier mobility due to the growth temperature should dominantly influence the decrease in the resistivity of our AZO films. Lin et al. reported that the change in the resistivity was mainly caused by the change in the carrier mobility in the AZO films derived by a sol–gel method [24]. Within our knowledge, the mobility is limited by several scattering mechanisms including grain boundary scattering, ionized impurity scattering, neutral impurity scattering and scattering at other defects and dislocations in poor crystallized area. The

Table 1 Summary of physical properties of AZO films deposited at different deposition temperature.

deposition temperature	R.T.	100 °C	200 °C	300 °C	400 °C	500 °C
resistivity (Ω cm)	0.44	0.25	0.18	0.12	0.022	0.0023
carrier mobility ($cm^2/V\,s$)	0.14	0.23	0.22	0.27	1.6	13
carrier concentration (10^{20} cm^{-3})	0.99	1.1	1.6	1.9	1.8	2.1
average transmittance (%)	89.9	90.6	90.7	90.7	90.0	91.9
calculated film density (g/cm^3)	4.45	4.7	4.9	5.0	5.3	5.9
critical angle (°)	0.295	0.305	0.306	0.305	0.312	0.334
calculated crystallite size (nm)	6.9	6.9	7.5	7.6	7.6	19
mean free path (nm)	0.026	0.044	0.048	0.062	0.38	3.2
FWHM of rocking curve (°)	19.8	19.6	14.5	8.89	5.79	2.26
optical band-gap (eV)	3.37	3.39	3.40	3.42	3.42	3.59

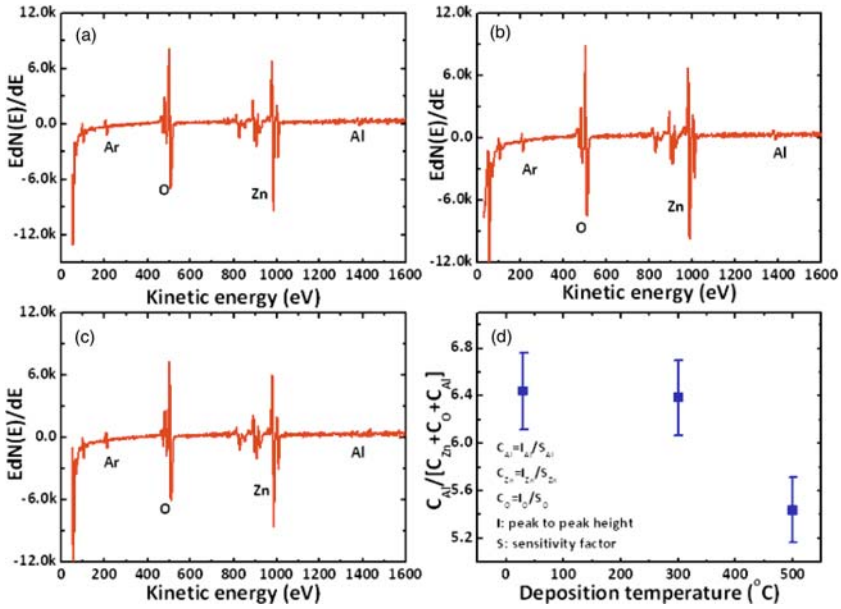

Figure 6 (online colour at: www.pss-a.com) Auger electron spectroscopy of each film deposited at (a) R.T., (b) 300 °C and (c) 500 °C and the relative Al composition calculated by these spectra.

dominant scattering in heavily doped AZO films would result from interstitial Al atoms in ZnO matrix rather than from grain boundaries since the mean-free-path of carriers is much less than the size of grains. Therefore, we confirm that the crystallographic quality and microstructure were of significant importance to achieve highly conductive oxides.

3.3 Optical properties High visible transmittance over 80% is an important criterion of transparent conducting oxides. The transmittance spectra of all samples as a function of wavelength are shown in Fig. 8. The average transmittance of all AZO films was approximately 90% in the wavelength ranging from 400 nm to 700 nm. The variation of transmission with wavelength is principally due to the inference phenomenon. As the growth temperature increased, the absorption edge shifted to the short wavelength (blue-shift). The cut-off behavior at the blue end of the optical absorption spectrum is determined by direct-electronic transition from the valance band to the conduction band. Thus, the direct optical band gap can be evaluated from transmission and reflectance data measured at short wavelengths. The theoretical relationship between E_g and an absorption coefficient can be expressed as [25]

$$(\alpha h\nu)^2 = A(h\nu - E_g), \tag{3}$$

where A is a function of the refractive index of the material, the reduced mass and the speed of light in vacuum, h is the Planck's constant, ν is the frequency of the radiation and E_g is an energy band gap (eV). A plot of $(\alpha h\nu)^2$ against the photon energy was used to obtain an optical band gap by using a linear fit and an extrapolation of the E_g value where $(\alpha h\nu)^2 = 0$. As the growth temperature increased, the

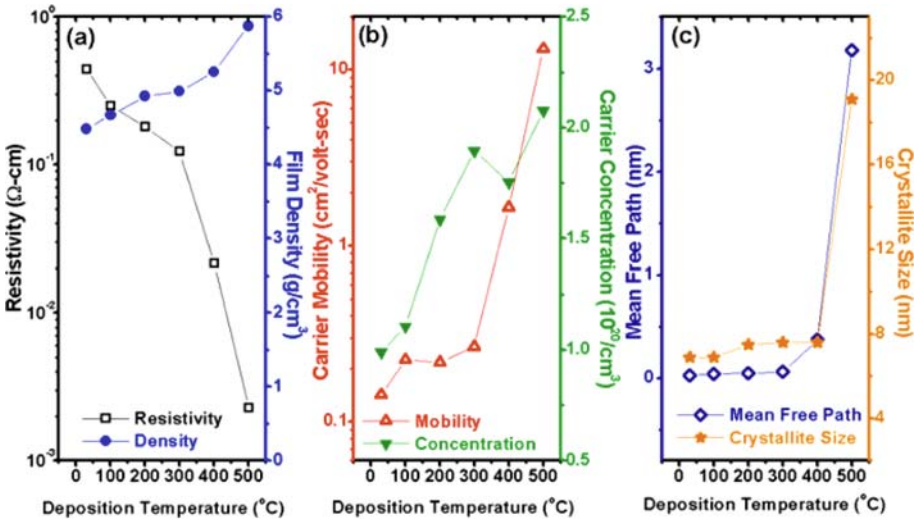

Figure 7 (online colour at: www.pss-a.com) Physical properties of AZO thin films as a function of deposition temperature, (a) resistivity and calculated film density, (b) carrier mobility and carrier concentration, (c) calculated mean free path of carrier and calculated crystallite size from rocking ω-scan.

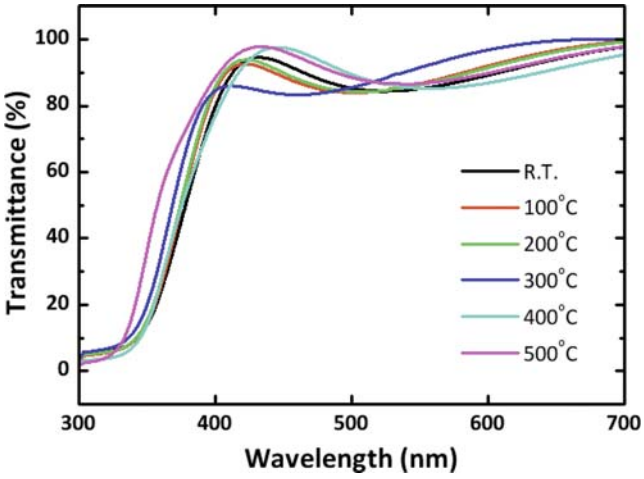

Figure 8 (online colour at: www.pss-a.com) Optical transmittance of AZO thin film, which were grown at different growth temperature.

optical band gap energy increased from 3.367 eV to 3.585 eV.

The optical band gap of undoped polycrystalline ZnO films is known as 3.28–3.30 eV at room temperature [24]. The change in the optical band gap of Al-doped ZnO films is mainly affected by two competing phenomena. One is the Burstein–Moss (BM) band-filling effect, which leads to a widening (blue shift) of the band gap with increasing carrier concentration [26, 27]. The other is many-body effects such as exchange energy due to electron–electron and electron-impurity interactions, which leads to a narrowing (red-shift) of the band gap when electron concentration exceeds the Mott critical value [28–30]. It should be noted that there are the competing effects of BM band-filling and band gap renormalization above the critical concentration. Recently, Lu et al. [31] reported that the sudden fall in energy gap occurred at $n_e \sim 5.4 \times 10^{19}$ cm^{-3}, which might be the onset of a semiconductor–metal transition. Above this concentration, the band gap increases again with a different rate due to the competing effects. Their theoretical formula based the perturbation theory fit our experimental data from RT to 300 °C of similar columnar structure well. However, a highly dense film (called honeycomb microstructure) may have more BM band-filling effect on the shift of optical band gap. In the further studies, we will investigate the relative contribution between BM band-filling effect and band gap renormalization on the optical band gap in different microstructures.

4 Conclusions Heavily-doped ZnO:Al films have been deposited on high temperature stable glass substrates using radio-frequency (RF) magnetron sputtering. The effect of growth temperature on physical properties of the films has been investigated. The microstructure evolved a columnar structure into a granular one with the increase in growth temperature and then a typical honeycomb-type microstructure representing huge grain formation and high densification was obtained. All Al-doped ZnO films exhibited high optical transparency and the absorption edge shifted to the short wavelength (blue-shift) as the growth temperature increased. The dense microstructure with a high crystallographic quality and large grains evolved at 500 °C enabled us to obtain 2.28×10^{-3} Ω cm and high visible transmittance over 90% even if the ZnO film was doped with an Al content of approximately 5.5 at%. It should be noted that a high crystallographic quality is of significant importance to obtain excellent transparent conductive oxides, especially in heavily doped oxides.

Acknowledgements This work was supported by the Korea Research Foundation grant (No. D00342), the Korea Science and Engineering Foundation (KOSEP) grant (No. R01-2007-000-10953-0) and the Ministry of Education, Science and Technology in Korea (project 'Brain Korea 21'). J. Hong was partially supported by the DIUS funded UK/Korea Focal Point Programme on Life Science.

References

[1] K. L. Chopra, S. Major, and D. K. Pandya, Thin Solid Films **102**(1), 1 (1983).
[2] S. A. Bashar and A. A. Rezazadeh, IEEE Trans. Microw. Theory Tech. **43**(9), 2299 (1995).
[3] B. G. Lewis and D. C. Pain, MRS Bull. **25**, 22 (2000).
[4] E. Fortunato, P. Barquinha, A. Pimentel, A. Goncalves, A. Marques, L. Pereira, and R. Martins, Thin Solid Films **487**, 205 (2005).
[5] E. Fortunato, D. Ginley, H. Hosono, and D. C. Paine, MRS Bull. **32**, 242 (2007).
[6] R. Waser (ed.), Nanoelectronics and Information Technology: Advanced Electronic Materials and Novel Devices (Wiley-VCH, 2003), pp. 917–972.
[7] A. L. Dawar and J. C. Joshi, J. Mater. Sci. **19**, 1 (1984).
[8] H. L. Hartnagel, A. L. Dawar, A. K. Jain, and C. Jagadish, Semiconducting Transparent Thin Films (Institute of Physics, Bristol, 1995).
[9] T. Minami, Thin Solid Films **516**, 5822 (2008).
[10] P. P. Sahay and R. K. Nath, Sens. Actuators B **133**, 222 (2008).
[11] Jianhua and R. G. Gordon, J. Appl. Phys. **71**(2), 880 (1992).
[12] T. Minami, H. Nanto, and S. Takta, Jpn. J. Appl. Phys. **23**, L280 (1984).
[13] B. H. Choi, H. B. Im, J. S. Song, and K. H. Yoon, Thin Solid Films **193/194**, 712 (1991).
[14] S. N. Qiu and I. Shih, Sol. Energy Mater. **15**, 261 (1987).
[15] B. D. Ahm, S. H. Oh, C. H. Lee, G. H. Kim, H. J. Kim, and S. Y. Lee, J. Cryst. Growth **309**, 128 (2007).
[16] K. Ellmer, J. Phys. D, Appl. Phys. **34**, 3097 (2001).
[17] T. Minami, Semicond. Sci. Technol. **20**, S35 (2005).
[18] E. Fortunato, D. Ginley, H. Hosono, and D. C. Paine, MRS Bull. **32**, 242 (2007).
[19] Handbook of Auger Electron Spectroscopy, Physical Electronics, 3rd ed. (Eden Psairie, 1976).
[20] C. R. Ottermann et al., Thin Solid Films **286**, 32 (1996).
[21] Philips Application Note: Reflectivity Measurements of Oxide Layers on Glass Surface (Netherlands).

[22] V. Holy, U. Piestch, and T. Baumbach, High Resolution X-ray Scattering from Thin Films to Lateral Nanostructures (Springer-Verlag, New York, 2004).
[23] T. Minami, T. Miyata, Y. Ohtani, and T. Kuboi, Phys. Status Solidi RRL **1**, R31 (2007).
[24] J.-P. Lin and J.-M. Wu, Appl. Phys. Lett. **92**, 134103 (2008).
[25] J. I. Pankove, Optical Processes in Semiconductors (Dover, New York, 1971).
[26] E. Burstein, Phys. Rev. **93**, 632 (1954).
[27] T. S. Moss, Proc. Phys. Soc. B **67**, 775 (1954).
[28] N. F. Mott, Philos. Mag. **6**, 287 (1961).
[29] P. A. Wolff, Phys. Rev. **126**, 405 (1962).
[30] D. Auvergne, J. Camassel, and H. Mathieu, Phys. Rev. B **11**, 2251 (1975).
[31] J. G. Lu, S. Fujita, T. Kawaharamura, H. Nishinaka, Y. Kamada, T. Ohshima, Z. Z. Ye, Y. J. Zeng, Y. Z. Zhang, L. P. Zhu, H. P. He, and B. H. Zhao, J. Appl. Phys. **101**, 083705 (2007).